


Utilization of Nitrogen-Doped Graphene Quantum Dots to Neutralize ROS and Modulate Intracellular Antioxidant Pathways to Improve Dry Eye Disease Therapy

Zixia Wu^{1,*}, Weibo Xia^{1,*}, Liling Ou¹, Ling Zheng¹, Bingying Hou¹, Tonghe Pan², Wenjie Sun¹, Leo H Koole¹, Yongqing Shao², Lei Qi¹ 

¹National Engineering Research Center of Ophthalmology and Optometry, Eye Hospital, Wenzhou Medical University, Wenzhou, 325027, the People's Republic of China; ²Ningbo Eye Hospital, Affiliated to Wenzhou Medical University, Ningbo, Zhejiang, 310000, the People's Republic of China

*These authors contributed equally to this work

Correspondence: Yongqing Shao, Ningbo Eye Hospital, Affiliated to Wenzhou Medical University, Ningbo, Zhejiang, 310000, the People's Republic of China, Tel +86-574 87862193, Email sunnieszq@163.com; Lei Qi, School of Ophthalmology & Optometry and Eye Hospital, Wenzhou Medical University, Wenzhou, Zhejiang, the People's Republic of China, 325027, Tel +86-577-88067973, Email imdoll@163.com

Purpose: Patients afflicted with dry eye disease (DED) experience significant discomfort. The underlying cause of DED is the excessive accumulation of ROS on the ocular surface. Here, we investigated the nitrogen doped-graphene quantum dots (NGQDs), known for their ROS-scavenging capabilities, as a treatment for DED.

Methods: NGQDs were prepared by using citric acid and urea as precursors through hydrothermal method. The antioxidant abilities of NGQDs were evaluated through: scavenging the ROS both extracellular and intracellular, regulating the nuclear factor-erythroid 2-related factor (Nrf2) antioxidant pathway of human corneal epithelial cells (HCECs) and their transcription of inflammation related genes. Furthermore, NGQDs were modified by Arg-Gly-Asp-Ser (RGDS) peptides to obtain RGDS@NGQDs. *In vivo*, both the NGQDs and RGDS@NGQDs were suspended in 0.1% Pluronic F127 (w/v) and delivered as eye drops in the scopolamine hydrobromide-induced DED mouse model. Preclinical efficacy was compared to the healthy and DPBS treated DED mice.

Results: These NGQDs demonstrated pronounced antioxidant properties, efficiently neutralizing free radicals and activating the intracellular Nrf2 pathway. *In vitro* studies revealed that treatment of H₂O₂-exposed HCECs with NGQDs induced a preservation in cell viability. Additionally, there was a reduction in the transcription of inflammation-associated genes. To prolong the corneal residence time of NGQDs, they were further modified with RGDS peptides and suspended in 0.1% Pluronic F127 (w/v) to create RGDS@NGQDs F127 eye drops. RGDS@NGQDs exhibited superior intracellular antioxidant activity even at low concentrations (10 µg/mL). Subsequent *in vivo* studies revealed that RGDS@NGQDs F127 eye drops notably mitigated the symptoms of DED mouse model, primarily by reducing ocular ROS levels.

Conclusion: Our findings underscore the enhanced antioxidant benefits achieved by modifying GQDs through nitrogen doping and RGDS peptide tethering. Importantly, in a mouse model, our novel eye drops formulation effectively ameliorated DED symptoms, thereby representing a novel therapeutic pathway for DED management.

Keywords: dry eye disease, antioxidant, nitrogen doped graphene quantum dots, Nrf2 antioxidant pathway

Introduction

Dry eye disease (DED) is a collective term for chronic and progressive ocular surface and tear disorders, which affects over 30% of the global population.¹⁻³ DED may arise from hindered tear production, excessive tear fluid evaporation, or contamination of the tear fluid. Individually or in combination, these factors can culminate in an irregular tear film composition and unstable osmolarity. DED symptoms encompass persistent dryness, eye irritation, stinging sensations,

fatigue, and visual disturbances. DED notably diminishes patients' quality of life, and exerts considerable pressure on health systems worldwide.⁴ Although the exact pathophysiology of the varied forms of DED remains unclear, it is evident that an accumulation of reactive oxygen species (ROS), including superoxide anion (O_2^-), hydrogen peroxide (H_2O_2), and hydroxyl radicals ($\cdot OH$), on the ocular surface is pivotal.⁵ This heightened ROS concentration denotes oxidative stress. Exacerbated oxidative stress in both the conjunctiva and tear fluid can instigate an inflammatory cascade, potentially initiating DED.^{6–8} Moreover, its prevalence escalates with aging and environmental exposures. Triggering environmental factors may include low humidity, atmospheric pollutants like ozone or microplastic residues⁹ to UV radiation, cosmetic eye products,¹⁰ and even electronic device usage.¹¹ Under typical conditions, biological antioxidant systems keep ROS in check; however, prolonged oxidative stress is known to disrupt the redox balance,^{12,13} leading to reduced lacrimal gland function and oxidative harm to crucial biomolecules, such as proteins, lipids, and nucleic acids. This disruption can ultimately halt cell growth or induce apoptosis.^{14–16}

Contemporary therapeutic strategies for DED predominantly center on enhancing tear quality or mitigating ocular surface inflammation using eye drops infused with corticosteroids or cyclosporine.¹⁷ However, these treatments are often limited by their low bioavailability. This limitation stems from factors such as reflexive blinking, the minimal volume of the tear film, and the nasolacrimal drainage flow.^{18–20} As a result, patients often require frequent doses (eg, 2 or 3 times daily) with heightened drug concentrations in the eye drop formulation. This extensive treatment approach can lead to undesirable systemic side effects and challenges in patient compliance. Excessive use of eyedrops can further elevate oxidative stress, exacerbating DED symptoms.²¹ Given these challenges, there is a persistent need for therapies that offer both enhanced safety and efficacy for DED.

Graphene quantum dots (GQDs), derived from fragments of graphene-based carbon materials, are renowned for their pronounced luminescence properties and commendable biocompatibility.^{22,23} The surface of GQDs show numerous defects and abundant unpaired electrons, attributes which are associated with reductive functional groups. Hence, GQDs hold significant promise as potent antioxidants.^{24–26} Notably, when GQDs are doped with heteroatoms such as nitrogen, their electron density is substantially augmented, bolstering their antioxidant capabilities.²⁷ Studies have illustrated the efficacy of GQDs in quenching ROS within biological systems, yielding promising results in mitigating gastric injuries²⁸ and reducing lipopolysaccharide-induced inflammation in macrophages.²⁹ As exceptional scavengers of intracellular ROS, GQDs present a promising avenue for addressing dry eye disease.

In this study, we engineered nitrogen-doped GQDs (NGQDs) that exhibited superior antioxidant efficacy both in vitro and within human corneal epithelial cells (HCECs). Additionally, the apoptosis rate in HCECs and the transcription of inflammation-associated genes diminished with NGQD intervention. Further investigations revealed that NGQDs neutralize intracellular ROS in the presence of H_2O_2 and activate the nuclear factor E2-related factor 2 (Nrf2) antioxidant pathway, safeguarding the cells. To improve bioavailability on the ocular surface, NGQDs were functionalized with RGDS (Arg-Gly-Asp-Ser) peptides. These peptides specifically target integrins on the corneal cell surface, enhancing the binding affinity of NGQDs to these cells. The resulting product was termed RGDS@NGQDs.^{30–32} Considering the physical barrier of the ocular mucosal layer, RGDS@NGQDs were dispersed in the amphiphilic solvent Pluronic F127 (0.1%), resulting in the formulation of RGDS@NGQDs F127 eye drops. The Pluronic F127 solvent, containing F127 PPO chains, can interact with ocular mucin proteins, enhancing the residence time of nanoparticles on the ocular surface. Its amphiphilic properties assist the nanoparticles in penetrating the cornea, further boosting their bioavailability.^{33–36} Our observations revealed that the RGDS@NGQDs F127 eye drops demonstrated superior intracellular antioxidant properties compared to unmodified NGQDs. In vivo experiments showed that the RGDS@NGQDs F127 eye drops markedly reduced ROS levels and mitigated symptoms associated with scopolamine hydrobromide-induced DED. These results suggest a promising strategy for devising DED treatments that counteract oxidative stress.

Materials and Methods

Reagents and Characterization

Chemical reagents for this study were sourced from Aladdin Co., Ltd., Shanghai, China, whereas laboratory consumables were acquired from Guangzhou Jet Bio-Filtration Co., Ltd., China. Specific reagents required for particular methods are detailed within the respective sections. The peptides used were synthesized by GL Biochem Ltd. (Shanghai, China). Cell

lines were procured from the American Type Culture Collection (ATCC, USA). Cell culture media and supplements were supplied by Gibco.

The structural and morphological characteristics of the NGQD derivatives were examined using high-resolution transmission electron microscopy (HRTEM, Talos F200X, Thermo Scientific, USA) and atomic force microscopy (AFM, Multimode 8, Bruker Co., Germany). Their chemical composition and elemental states were analyzed using X-ray photoelectron spectroscopy (XPS, Thermo Escalab 250Xi, USA). Ultraviolet-visible (UV-Vis) and fluorescence spectra of the NGQD derivatives were recorded using an Agilent Cary 100 spectrophotometer (USA) and a Hitachi 7000 fluorescence spectrophotometer (Japan), respectively. Fourier transform infrared (FT-IR) spectra were obtained using a Thermo Nicolet 6700 spectrometer (USA). The surface zeta potential of NGQDs and their derivatives were measured by dynamic light scattering (DLS) at room temperature using a Zetasizer Nano system (Malvern ZS90).

Synthesis of NGQDs

NGQDs were synthesized following a previously outlined method.³⁷ Specifically, we dissolved 0.88 g of citric acid and 1.08 g of urea in 15 mL of distilled water (DI H₂O). This solution was then subjected to a hydrothermal process in a 25 mL Teflon-lined stainless-steel autoclave, maintained at 160 °C for 4 hours. Following this, the preliminary product was subjected to tube dialysis (molecular weight retention range: 500–1000 Da, sourced from Shanghai Yuanye Bio-Technology Co., Ltd, China) for 24 hours, to eliminate unincorporated small molecules. The resulting purified NGQDs were then freeze-dried to yield a powder, which was used in further investigations.

·OH Consumption Capacity with the TMB Method

3,3',5,5'-Tetramethylbenzidine (TMB, 2 mM), horseradish peroxidase (HRP, 0.1 U/mL) and H₂O₂ (1 mM) were first mixed to produce ·OH. Subsequently, different concentrations of NGQDs were added dropwise into the TMB mixture. The color changes of the mixture were recorded by picture and video. The ability to consume hydroxyl radicals (·OH) was monitored through measurement of the UV-Vis absorbance of TMB cation radicals at 652 nm after 10 minutes. The antioxidant capacity was presented as the percentage of $(OD_{\text{control}} - OD_{\text{sample}}) / OD_{\text{control}}$ (the control group is the mixture of TMB, HRP, and H₂O₂).

Total Antioxidant Capacity of NGQDs with the FRAP Method

The total antioxidant capacity of the NGQDs was determined by assessing the ferric reducing ability of plasma using a standard kit (FRAP, Beyotime, China). Antioxidants reduce the colorless Ferric-tripyridyltriazine (Fe³⁺-TPTZ) to the blue Fe²⁺-TPTZ. The UV-Vis absorbance of Fe²⁺-TPTZ at 593 nm was therefore used to monitor the antioxidant capacity. Following the instruction manual, an FeSO₄·7H₂O standard curve was first prepared. The total antioxidant capacity was expressed by the concentration of the Fe₃SO₄ standard solution. The reaction temperature was 37 °C, and the reaction time was 8 min.

In vitro Cytocompatibility Studies

HCECs were cultured in DMEM/F12 growth medium, supplemented with 10% (v/v) certified fetal bovine serum (FBS) and 50 µg/mL gentamicin. The culture was maintained in an environment with 10% CO₂ at a constant temperature of 37 °C.

Cell viability was assessed using a CCK-8 assay kit from Dojindo. Initially, cells were seeded at a density of 5,000 cells per well in 96-well plates and incubated for 24 hours in standard growth medium. Following this, the medium in each well was replaced with 100 µL of fresh medium, containing varying concentrations of NGQD derivatives or H₂O₂. After incubation for a designated duration, cells were subjected to the CCK-8 assay, in accordance with the manufacturer's instructions. The absorbance at 450 nm was measured using a SpectraMax 190 microplate reader (Molecular Devices, USA). Cell viability is presented as a percentage relative to the control group, which was maintained in regular growth medium.

Living and dead cells were distinguished using a calcein-AM/PI Double Staining Kit from Dojindo. Cells were plated at a density of 20,000 cells per well in 24-well plates, and incubated for 24 hours in standard growth medium. Subsequently, the medium was replaced with fresh medium containing varying concentrations of NGQD derivatives or H₂O₂, followed by incubation for an appropriate duration. After washing thrice with PBS, the cells were stained with

calcein-AM or PI, according to the manufacturer's protocol, and incubated at 37 °C for 15 minutes. Cell visualization was performed using a fluorescence microscope (OLYMPUS IX81), equipped with green and red fluorescent exciters (Excitation/Emission wavelengths for calcein-AM: 490/515 nm; for PI: 535/617 nm).

Intracellular Antioxidant Capacity Evaluation

HCECs were divided into different groups, including the negative control group (NC), oxidative stress group (H_2O_2), NGQD derivative-treated group (NGQDs or RGDS@NGQDs) and NGQD derivative antioxidant group ("NGQDs+ H_2O_2 " or "RGDS@NGQDs+ H_2O_2 "). First, all the cells were cultured in regular medium for 24 h. At 24 h after seeding, the culture medium of the NC group and H_2O_2 group was changed to fresh medium, while the other two groups were changed to fresh medium with different concentrations of NGQD derivatives and incubated for 24 h. Subsequently, the culture medium of the oxidative stress group and NGQD derivative antioxidant group was changed to medium containing no FBS in addition to H_2O_2 (400 μ M) and cultured for another 4 h. The cell viability of HCECs was finally determined by CCK-8 assay.

Apoptosis Determination

The apoptosis assay for HCECs was conducted using the FITC Annexin V Apoptosis Detection Kit I, following the instructions provided by BD Biosciences (San Jose, CA, USA). HCECs were cultured in 6-well plates at a density of 200,000 cells per well. Following the treatment protocols detailed in Section 2.6, the cells were trypsinized and then resuspended in binding buffer. For staining, 10 μ L of FITC Annexin V and 10 μ L of PI were added to the cells, which were then incubated for 15 minutes at room temperature in the dark. The assessment of apoptosis was carried out using flow cytometry (FACSCalibur, BD Biosciences).

Intracellular ROS Detection

Intracellular ROS levels were measured using a Reactive Oxygen Species Assay Kit from Beyotime. Cells were seeded at a density of 20,000 cells per well in 24-well plates. These cells were grouped and treated according to the procedures outlined in Section 2.6. Post-treatment, the cells were rinsed with FBS-free medium. To detect ROS, 10 μ M of the ROS probe 2'-7'-dichlorofluorescein diacetate (DCFH-DA) was added to each well, followed by incubation for 20 minutes. Subsequently, the cells were washed three times with serum-free medium, and then observed under a fluorescence microscope, using a green fluorescent exciter.

Western Blot

HCECs were cultured in 6-well tissue culture plates, at a seeding density of 200,000 cells per well, and incubated for 24 hours. The cells were categorized into different groups and subjected to treatments, as detailed in Section 2.6. Post-treatment, the cells were lysed using western cracking buffer (Beyotime) to extract total protein. The concentration of the total protein was quantified using the BCA Protein Assay Kit (Thermo). Western blot analysis was then performed to assess the expression levels of Nrf2 and Keap1 using rabbit polyclonal antibodies (ab62352, ab227828, Abcam). β -Tubulin (AF1216, Beyotime) served as the loading control. The intensities of the bands were quantified using Image Lab software (Bio-Rad Laboratories, Inc.), and normalized against the β -tubulin band.

Immunofluorescence

The cells from various groups were cultured on 10×10 mm slides in a 24-well plate, where each slide contained 20,000 cells, for 24 hours. The cells were categorized into four groups: the NC group, the oxidative stress group (treated with 400 μ M H_2O_2), the NGQD-treated group (treated with 50 μ g/mL NGQDs), and the NGQD antioxidant group (treated with 50 μ g/mL NGQDs and 400 μ M H_2O_2). Treatment protocols were performed as outlined in Section 2.6. After treatment, cells were fixed in cold methanol for 5 minutes at -20 °C, followed by blocking with 3% w/v BSA for 1 hour at room temperature. Subsequently, the cells were incubated with the anti-Nrf2 antibody (ab62352, Abcam) for 24 hours at 37 °C. After incubation with a FITC-tagged secondary antibody (A16024, Thermo, Ex/Em: 495/515 nm), cell nuclei were stained with DAPI (C1005, Beyotime, Ex/Em: 340/488 nm) for 2–5 minutes. Finally, the slides were examined using confocal laser scanning microscopy (CLSM, Zeiss LSM880).

In vitro Expression of Inflammation-Related Factors

The expression levels of inflammation-related mRNA in HCECs were determined using reverse transcription-polymerase chain reaction (RT-PCR). Cells were plated in 6-well plates at a density of 200,000 cells per well and categorized into four groups: the NC group, the oxidative stress group (treated with 400 μ M H₂O₂), the NGQD-treated group (treated with 50 μ g/mL NGQDs), and the NGQD antioxidant group (treated with both 50 μ g/mL NGQDs and 400 μ M H₂O₂). RNA from each group was extracted using TRIzol, with quality and purity assessed by the ratios of A260/A280 (between 1.8 and 2.0) and A260/A230 (greater than 2.0). Complementary DNA (cDNA) was synthesized from high-purity RNA using the HiScript III RT SuperMix for qPCR (+gDNA wiper) kit (Vazyme, China). The relative expression of IL-1 β (5'-ATGATGGCTTATTACAGTGGCAA-3' and 5'-GTCGGAGATTCGTAGCTGGA-3'), IL-6 (5'-AAATCACCATGCACCTCATCC-3' and 5'-AGAGGATTGTGCCCCGAACTAAA-3'), IL-8 (5'-ATGCTTTTGATCTGCACAGCTGCAC-3' and 5'-TGGTCCAGCAGGAATAACCCTCAG-3'), TNF- α (5'-GTTCCCCAGGGACCTCTCTC-3' and 5'-GGCTACAGGCTTGTCACCTCG-3'), and IFN- γ (5'-TCGGTAACTGACTTGAATGTCCA-3' and 5'-TCGCTTCCCTGTTTTAGCTGC-3') were analyzed using RT-PCR. All gene mRNA expression was normalized to the expression of GAPDH (5'-ATGTTTCGTCATGGGTGTGAA-3' and 5'-GGTGCTAAGCAGTTGGTGGT-3'). The fold change in expression across various groups was calculated using the $2^{-\Delta\Delta C_t}$ method, where ΔC_t is defined as the C_t value of the target gene minus the C_t value of GAPDH (housekeeping gene). The relative mRNA levels were determined by comparing the ratio of $2^{-\Delta\Delta C_t}$ of the treated group to that of the NC group.

Preparation and Characterization of RGDS@NGQDs F127 Eye Drops

First, EDCI (28.8 mg) and NHS (34.5 mg) were dissolved in 5 mL of DI H₂O. RGDS (Arg-Gly-Asp-Ser) peptides (5 mg) were added to the EDCI/NHS solution and mixed for 1 h at 37 °C, which activated the carboxyl of RGDS peptides. Subsequently, the activated RGDS was mixed with NGQDs (7.15 mg/mL, 5 mL) and reacted at 37 °C overnight. The crude product was dialyzed in a dialysis tube (retained molecular weight: 500–1000 Da, Shanghai Yuanye Bio-Technology Co., Ltd, China.) for 24 h to remove all unreacted small molecules. The purified RGDS@NGQDs were freeze-dried and resuspended in 0.1% Pluronic F127 (w/v) to obtain RGDS@NGQDs F127 eye drops.

Cellular Uptake Assay

HCECs were cultured on 10×10 mm slides within a 24-well plate at a density of 30,000 cells per slide. Following a 24 h period, the culture medium was replaced with fresh medium containing either NGQDs or RGDS@NGQDs (200 μ g/mL), and the cells were incubated for either 0.5 or 2 hours. Subsequently, the cells were gently rinsed three times with PBS and then fixed using 4% paraformaldehyde. The cell nuclei were stained using 7-AAD (Invitrogen, Ex/Em: 546/647 nm). Fluorescence images were captured using a confocal laser scanning microscopy. The fluorescence intensity was evaluated by the software of image J.

In vivo Therapeutic Effects of RGDS@NGQDs F127 Eye Drops

Healthy male C57BL/6 mice, aged 6–8 weeks, were procured from Shanghai SLAC Laboratory Animal Co., Ltd. All mice were housed at the Laboratory Animal Center of Wenzhou Medical University, where all animal care and experimental procedures were conducted in strict adherence to the guidelines set by the Laboratory Animal Ethics Committee of Wenzhou Medical University. This center operates under the experimental animal license SYXK (Zhejiang) 2015–0009, ensuring compliance with established experimental standards. All animal welfare and experimental protocols rigorously followed the ethical guidelines as stipulated in the “Laboratory Animal-Guidelines for Ethical Review of Animal Welfare” of China (GB/T 35892–2018). The experimental methods and research protocol of this study have been approved by the Laboratory Animal Ethics Committee of Wenzhou Medical University (wydw 2021–0302).

Prior to the commencement of the experiments, the eyes of all mice were thoroughly examined using slit-lamp microscopy (SLM-7E, KANGHUA, China), to ensure the selection of eyes free from infection or noticeable anterior segment abnormalities for subsequent tests. The mice were randomly allocated into four groups, with each group comprising six mice: 1) a normal healthy control group; 2) DED mice treated with PBS; 3) DED mice treated with NGQDs F127 (50 μ g/mL) eye drops; and 4) DED mice treated with RGDS@NGQDs F127 (50 μ g/mL) eye drops. To induce the DED model, scopolamine hydrobromide (0.2 mL, 2.5 mg/mL) was administered subcutaneously to the mice four times daily over 7 days. Concurrently,

the ocular surface of the mice was treated with one drop (5 μ L) of either PBS or the respective eye drops, also four times daily for 7 days.

On days 1 and 7, corneal fluorescein staining scores were assessed to evaluate the integrity of the cornea. For this procedure, 1 μ L of 0.05% sodium fluorescein solution was instilled into the lower conjunctival sac and left to interact for 2 minutes. Subsequently, the eyes were examined using a slit lamp equipped with a cobalt blue filter. The cornea was divided into four quadrants for scoring, based on the extent of fluorescein uptake, as follows: 0, no noticeable fluorescent spots; 1, micropunctate staining with fewer than 30 spots; 2, more than 30 punctate stains without diffuse staining; 3, diffuse staining but without positive plaque; and 4, severe plaque or patch staining. The final corneal fluorescein staining score was the aggregate of the scores from all four quadrants.

After seven days of treatment, the mice were humanely euthanized, and eyes were harvested for analysis. For histological examination, eyes were fixed in 10% formalin, followed by dehydration, cross-sectioning, and staining using hematoxylin and eosin (H&E) and periodic acid-Schiff (PAS) following standard protocols. The morphology of the corneal and goblet cells was then observed under a microscope. For the assessment of ROS content, the eyes were rapidly frozen in liquid nitrogen and sectioned to a thickness of 10 μ m. These sections were stained with DAPI for nuclear visualization and with dihydroethidium (DHE), a fluorescence probe that is oxidized by ROS to form a red fluorescent product (Ex/Em: 535 nm/610 nm). For corneal immunofluorescence staining, eyeballs were fixed, dehydrated, frozen, and sectioned into 10 μ m thick slices. After being rinsed three times with PBS, the slices were incubated in 0.3% Triton X-100 for 10 min and then 10% goat serum for 1 h at room temperature. Subsequently, the sections were incubated with the primary antibody at 4 °C overnight, followed by appropriate fluorescence-conjugated secondary antibodies at room temperature for 2 h. The stained sections were subsequently observed using a fluorescence microscope.

Statistical Analysis

For all datasets obtained from replicate experiments, we computed the mean and standard deviation. When the data conformed to a normal distribution, significant differences (p-values) were assessed through one-way analysis of variance (ANOVA) complemented by Tukey's multiple comparison test, utilizing GraphPad Prism version 7.00 (GraphPad Software, USA). The levels of significance were indicated as follows: a single asterisk (*) represents $p \leq 0.05$, double asterisks (**) denote $p \leq 0.01$, and triple asterisks (***) signify $p \leq 0.001$. A p-value of ≤ 0.05 was considered statistically significant.

Results

Physical Characterization and Antioxidant Evaluation of NGQDs

Utilizing citric acid and urea as precursors, we synthesized nitrogen-doped GQDs (NGQDs) through a hydrothermal method. HRTEM imaging revealed that NGQDs are spherical, with an average diameter of 3.5 ± 1.2 nm (based on a count of 100 NGQDs), as shown in [Figure 1a](#). AFM measurements indicated that their thicknesses predominantly range between 2 and 3 nm, averaging 2.04 ± 1.24 nm, which corresponds to approximately 9 layers (see [Figure S1a](#)). XPS analyses confirmed the presence of C (284 eV), N (400 eV), and O (533 eV) in the NGQDs, with respective concentrations of 51.57%, 10.03%, and 38.4% ([Figure 1b](#)). The high-resolution XPS C1s spectrum displayed peaks corresponding to C=C (284.7 eV), C-N (285.9 eV), and C=O (288.5 eV) bonds, whereas the N1s spectrum presented peaks related C-N-C (399.9 eV) and N-H (401.6 eV) (refer to [Figure S1b](#) and [c](#)). The effective zeta potential of NGQDs was determined as -30.2 . As deduced from the UV-Vis spectrum ([Figure 1c](#)), the absorption peak at 236 nm can be attributed to the C=C bond, and the peak at 331 nm is linked to the C=O bond. The photoluminescence spectrum indicates maxima at excitation and emission wavelengths of 360 nm and 460 nm, respectively ([Figure 1c](#)). Surface functional groups on NGQDs were identified using the FT-IR spectrum ([Figure 1d](#)). A prominent stretching vibration at 3453 cm^{-1} was discerned, corresponding to the N-H or O-H groups. Vibrations at 1548 cm^{-1} and 1023 cm^{-1} were ascribed to the bending motions of N-H and C-N, respectively, while the band at 1637 cm^{-1} stemmed from the C=C bond's bending vibration. These findings demonstrate that NGQDs are layered quantum dots, enriched with NH functional groups, a conclusion aligning with our earlier publication.³⁷

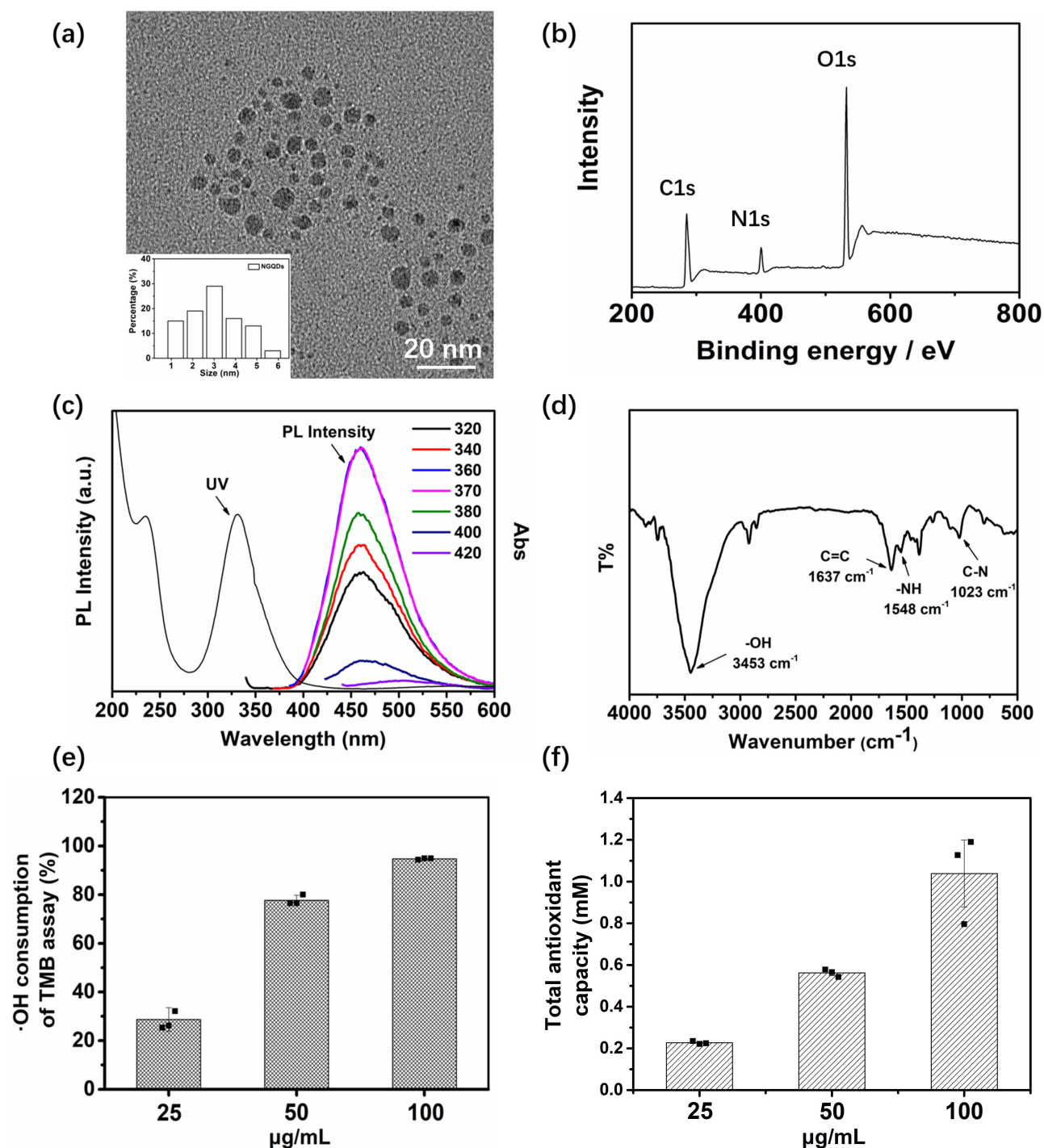


Figure 1 Characterization of NGQDs and their antioxidant capacity. (a) HRTEM image of NGQDs (Inset: the size distribution of NGQDs); (b) XPS full survey of NGQDs; (c) the UV-Vis and photoluminescent spectrum of NGQDs; (d) the FT-IR spectrum of NGQDs; (e) the $\cdot\text{OH}$ consumption capacity of NGQDs; (f) the total antioxidant capacity of NGQDs.

The antioxidant potential of NGQDs was initially evaluated using the TMB assay. To begin, TMB, H_2O_2 , and HRP were combined. In this blend, the colorless TMB can undergo oxidation, resulting in the formation of cationic TMB radicals (oxTMB, blue) due to the presence of $\cdot\text{OH}$. Following this, varying concentrations of NGQDs were gradually introduced into the mixture. The color transition of the mixture was documented in a video ([Video 1](#)). In the video, the concentrations of NGQDs were 1.77, 1.43, 1.08, 0.73, 0.37, 0.19, and 0 mg/mL from left to right. With the addition of NGQDs, the blue

color of oxTMB gradually faded. The fading rate was positively correlated with the concentration of NGQDs, indicating that NGQDs consumed the produced $\cdot\text{OH}$. The UV–Vis absorbance of oxTMB at 652 nm was further used to monitor the $\cdot\text{OH}$ consumption capacity of NGQDs (Figure 1e). The capacity to consume $\cdot\text{OH}$ was computed using the formula: $(\text{OD}_{\text{control}} - \text{OD}_{\text{sample}})/\text{OD}_{\text{control}}$, in which the control group comprises a mixture of TMB, HRP, and H_2O_2 . We observed that as the NGQD concentration increased, the $\cdot\text{OH}$ neutralization rate rose correspondingly. Additionally, to assess the total antioxidant potential of NGQDs—which encompasses the neutralization of $\cdot\text{OH}$, O_2^- , and H_2O_2 —the FRAP assay was employed. Initially, the standard curve for $\text{FeSO}_4 \cdot 7\text{H}_2\text{O}$ was established, yielding the equation $y = 0.3026x + 0.058$ (refer to Figure S2). Subsequently, varying concentrations of NGQDs were combined with Fe^{3+} -TPTZ. During this process, NGQDs facilitated the reduction of Fe^{3+} -TPTZ to Fe^{2+} -TPTZ. The UV–Vis absorption of the resulting Fe^{2+} -TPTZ at 593 nm was tracked. This data was then used to determine the antioxidant capacity (in mM) based on the Fe_3SO_4 standard solution (see Figure 1f). As the concentration of NGQDs increased, their overall antioxidant capacity also rose. These findings suggest that NGQDs act as antioxidants with the capability to neutralize ROS, indicating their potential for application in DED treatment.

Cytocompatibility and Intracellular Antioxidant Capacity of NGQDs

We assessed the cytocompatibility of NGQDs using the CCK-8 assay (Figure 2a). HCECs were exposed to various concentrations of NGQDs for time durations of 24, 48, and 72 h. Remarkably, cell viability remained above 90% throughout the 72-hour incubation period when NGQDs concentrations were maintained at or below 50 $\mu\text{g/mL}$. However, when the concentration reached 100 $\mu\text{g/mL}$ of NGQDs, cell viability was above 80% at both 24 and 48 h but decreased to 74.8% by the 72-hour mark. Further insights into the cytocompatibility of NGQDs were garnered using the Living/Dead cell double staining kit, as shown in Figure S3. In alignment with the CCK-8 assay results, HCECs were subjected to different concentrations of NGQDs across intervals of 24, 48, and 72 h. These were subsequently stained with calcein-AM/PI. Intriguingly, at NGQD concentrations reaching up to 50 $\mu\text{g/mL}$, an observable increase in cell proliferation was seen with longer culture durations, as evidenced by the calcein-AM staining. This indicates that NGQDs, within this concentration range, did not impede cell growth. Conversely, at a concentration of 100 $\mu\text{g/mL}$ NGQDs, cell density remained consistent over the duration. It is worth noting that some degree of cell mortality was observed, as indicated by the PI staining. These observations underscore the commendable cytocompatibility of NGQDs, but indicate that they can still manifest mild cytotoxic effects when cells encounter elevated NGQDs concentrations for prolonged periods.

We further examined the intracellular antioxidant characteristics of NGQDs, as illustrated in Figure 2b. We induced oxidative stress by subjecting cells to H_2O_2 at a concentration of 400 μM . This exposure resulted in a marked reduction in cell viability, dropping to approximately 38.6%. However, when cells were pre-treated with NGQDs before H_2O_2 exposure, their survival rates significantly increased. Specifically, cells pre-treated with NGQDs at concentrations of 50 and 100 $\mu\text{g/mL}$ for 24 h, followed by H_2O_2 exposure, showed survival rates of above 75%, respectively.

Flow cytometry was employed to analyze the apoptosis of HCECs, further elucidating the intracellular antioxidant potential of NGQDs. In the group exposed to H_2O_2 , a pronounced increase in late apoptotic cells was observed, comprising 10.2% (refer to Figure 2c). Nevertheless, when cells were pre-treated with NGQDs at a concentration of 50 $\mu\text{g/mL}$ for 24 h before being exposed to H_2O_2 , the rate of late apoptosis was significantly reduced, showing a twofold decrease to 5.33%. These findings underscore the antioxidant properties of NGQDs. Yet, as shown in Figure 2a, higher concentrations of NGQDs did exhibit some cytotoxic effects on HCECs. Considering the data on intracellular antioxidant abilities, it is conceivable that the cytotoxicity induced by NGQDs may be linked to an excessive antioxidant action, which could disrupt the redox equilibrium within the cells.

Cells generate ROS following H_2O_2 exposure, posing a threat to vital cellular components and potentially causing cell death. Hence, monitoring intracellular ROS levels is pivotal in gauging the antioxidant efficacy of NGQDs. For this purpose, we utilized the DCFH-DA method to quantify intracellular ROS. ROS has the ability to oxidize DCFH-DA, leading to the formation of DCF, which emanates green fluorescence. As illustrated in Figure 2d, a prominent green fluorescence was evident in the H_2O_2 -exposed group, indicating elevated ROS production. In contrast, cells pre-treated with NGQDs prior to H_2O_2 exposure demonstrated a significant decline in ROS fluorescence. Moreover, cells exclusively

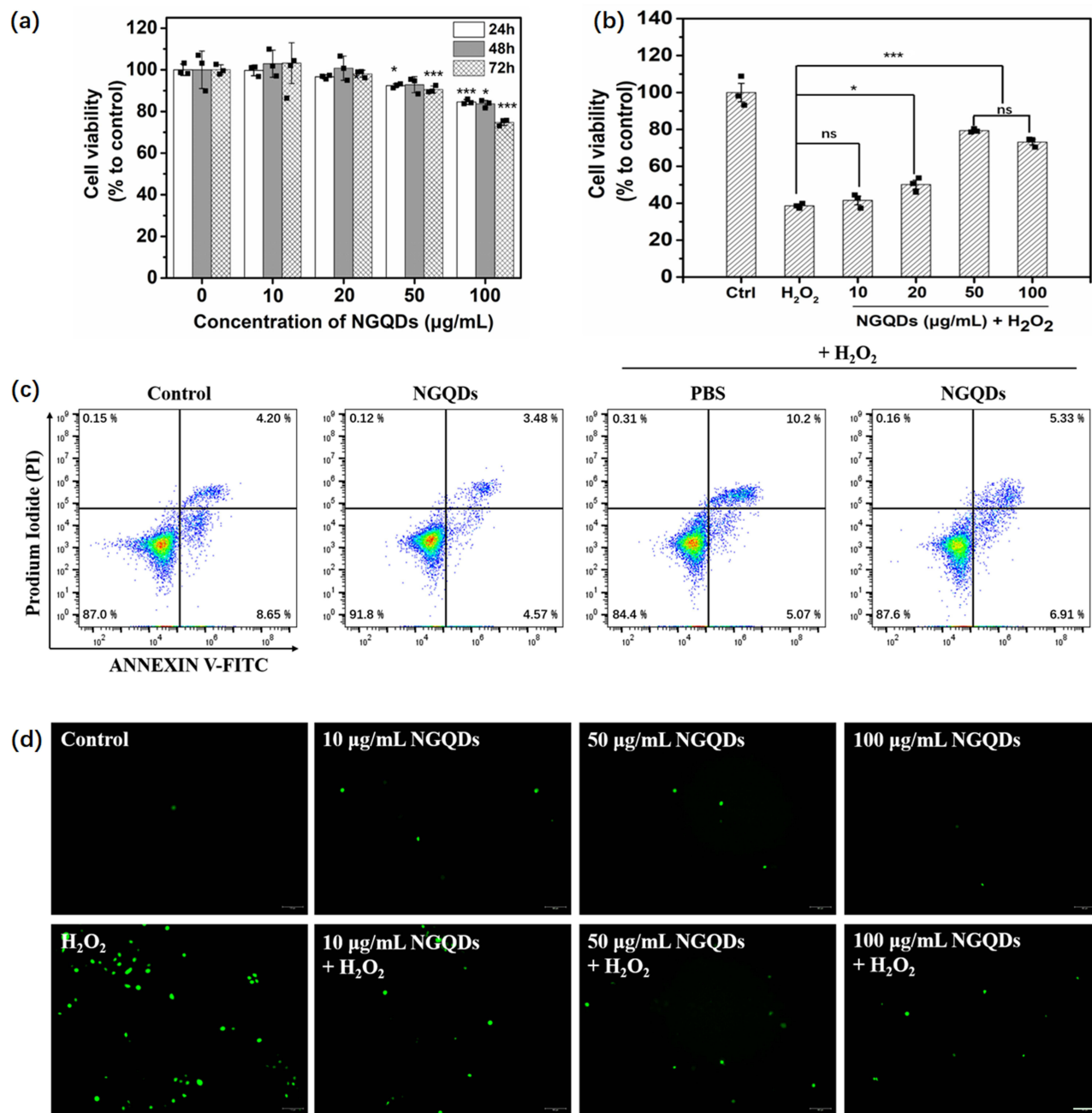


Figure 2 Cytocompatibility and intracellular antioxidant capacity of NGQDs. (a) The cell viability of NGQD-treated HCECs, as assessed by CCK-8 assay (* $p \leq 0.05$, *** $p \leq 0.001$ vs the NGQDs (0 $\mu\text{g/mL}$)-treated group in the same time period); (b) The antioxidant capacity of NGQDs, as assessed by CCK-8 assay (ns. $p > 0.05$, * $p \leq 0.05$, *** $p \leq 0.001$ vs the corresponding treatment group linked with it); (c) Flow cytometry analysis of cell apoptosis with different treatments (The flow cytometry plots are divided into four quadrants: the upper left quadrant indicates dead cells, the upper right quadrant shows late apoptotic cells, the lower left quadrant represents non-apoptotic cells, and the lower right quadrant indicates early apoptotic cells); (d) ROS detection in HCECs by DCFH-DA probes; the scale bar represents 100 μm .

exposed to NGQDs showed negligible ROS fluorescence. Together, these results highlight that NGQDs effectively neutralize intracellular ROS, thus emphasizing their role in antioxidant defense and enhancing cell protection.

Effects of NGQDs on Nrf2/Keap1 Gene Expression in HCECs

The above findings suggest that NGQDs protect cells from intracellular oxidative stress by mitigating excessive ROS. This led us to speculate about NGQDs' potential role in modulating the cellular antioxidant signaling pathway. To explore this further, we examined the impact of NGQDs on the expression of the Nrf2/Keap1 pathway, a cornerstone in

defending against environmental oxidant challenges.³⁸ Nrf2 is a transcription factor sensitive to redox changes, which is regulated by Keap1. Under normal conditions, Nrf2 is kept inactive due to ubiquitination by a cul3-based E3 ligase, resulting in its binding by Keap1. However, during oxidative stress, the cysteine residues in Keap1 deactivate the ligase, releasing Nrf2. Once freed, Nrf2 translocates to the nucleus, instigating the production of antioxidant enzymes, such as superoxide dismutase. In extreme oxidative stress situations, a spike in ROS may cause DNA damage and cell apoptosis. This challenging condition can subsequently hamper Nrf2 expression.³⁹

We examined Nrf2 and Keap1 expression using WB. Cells were exposed to H₂O₂ (400 μ M) for 4 h to establish the oxidative stress group (H₂O₂ group). In the presence of oxidative stress, the Nrf2 expression in the group treated with NGQDs (50, 100 μ g/mL) and then subjected to H₂O₂ (NGQDs+ H₂O₂ group) showed a significant upregulation in comparison to the H₂O₂ group alone. This elevation was concentration-dependent (Figures 3a, S4a and Figures 3c, S4b).

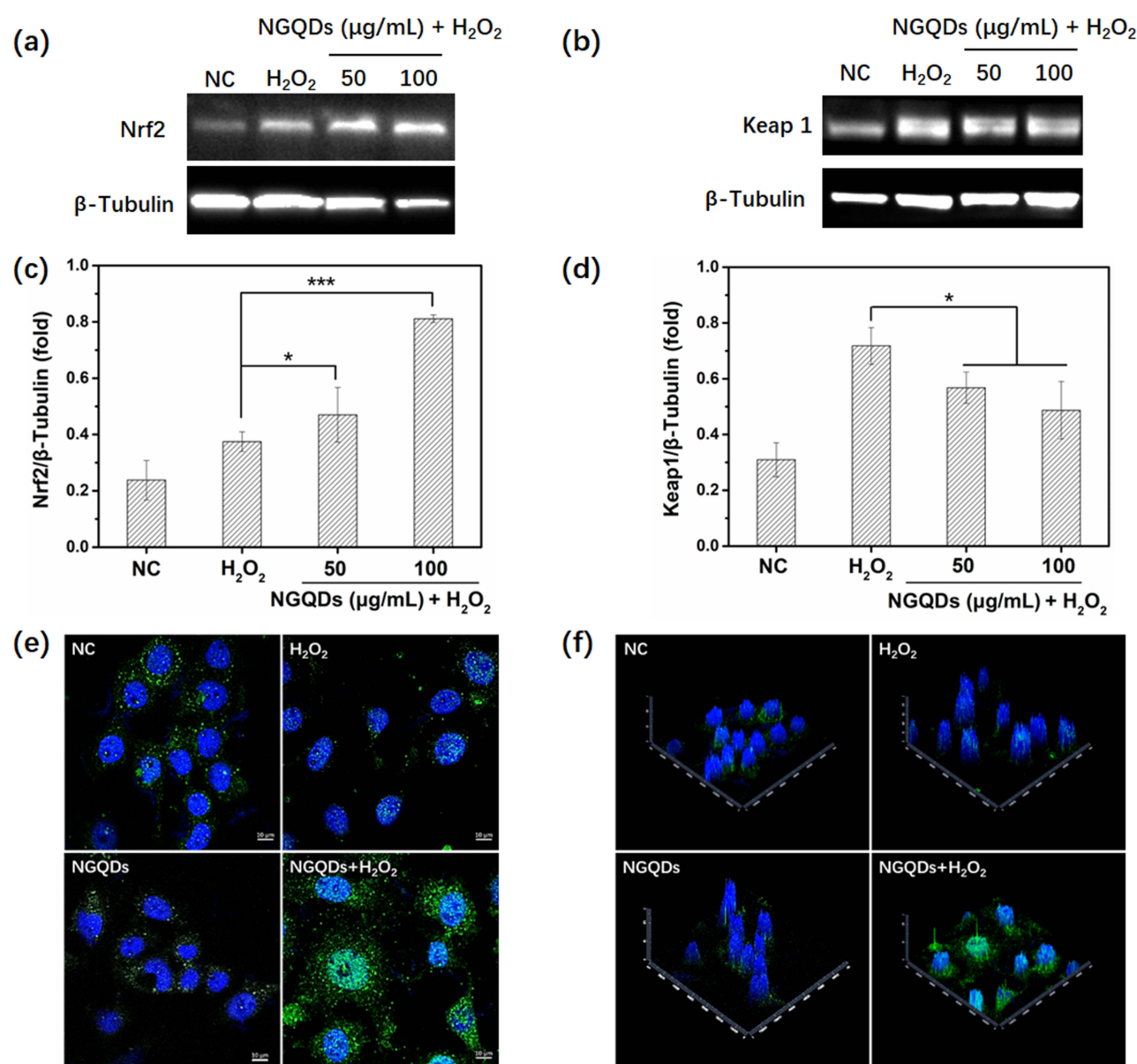


Figure 3 Influence of NGQDs on the Nrf2/Keap1 gene expression in HCECs. (a and b) Nrf2 and Keap1 expression assessed by WB (The original images were presented in Figure S4a); (c and d) Relative expression levels of Nrf2 and Keap1 (The three repeats of WB image against Nrf2 or Keap1 protein were presented in Figures S4b and 4c); (e) Visualization of Nrf2 expression by immunofluorescence. Images showing a composite of green fluorescence from the FITC-tagged secondary antibody and blue from DAPI-stained nuclei. Scale bars represent 10 μ m; (f) The 3D top-down view of e. (* $p \leq 0.05$, *** $p \leq 0.001$ vs the corresponding treatment group linked with it).

Given the strikingly high late apoptosis rate of 10.2% in the H_2O_2 group (as seen in Figure 2c), we surmised that the suppressed Nrf2 expression in the H_2O_2 group arises from cell apoptosis. In parallel, Keap1 expression appeared inversely proportional to that of Nrf2, pointing to the modulatory role of Keap1 in Nrf2 expression (refer to Figures 3b, S4a and Figures 3d, S4c). The WB data suggests that NGQDs efficiently neutralize the majority of cellular ROS when faced with oxidative stress. This action reduces the cell apoptosis rate and triggers the Nrf2 antioxidant pathway, consequently enhancing cellular survival. Expanding upon our earlier point that Nrf2 relocates to the nucleus during oxidative stress, we used immunofluorescence to examine Nrf2's expression and positioning. Figure 3e illustrates a pronounced increase in Nrf2 expression in the NGQDs (50 $\mu\text{g/mL}$) + H_2O_2 group relative to other groups, evident from the green fluorescence. Notably, the majority of this Nrf2 was found within the nucleus. The 3D renderings of Figure 3e further corroborate Nrf2's nuclear translocation in the NGQDs+ H_2O_2 group (Figure 3f).

Effects of NGQDs on the Transcription of Inflammation-Related Genes Under Oxidative Stress

Inflammation and oxidative stress are intricately interconnected. To explore this association, we evaluated the expression patterns of genes linked to inflammation in HCECs subjected to oxidative stress conditions, as detailed in Figure 4. Exposure to H_2O_2 markedly increased the transcription levels of key inflammatory mediators, including interleukin-1 β (IL-1 β), interleukin-6 (IL-6), tumor necrosis factor- α (TNF- α), interleukin-8 (IL-8), and interferon- γ (IFN- γ). This finding substantiates the hypothesis that oxidative stress triggers a robust inflammatory response. Notably, when NGQDs were co-treated with H_2O_2 , we observed a significant reduction in the expression of these inflammatory genes. This suggests that NGQDs have antioxidative properties, capable of neutralizing oxygen free radicals and reducing inflammation in HCECs. Additionally, treating HCECs solely with NGQDs did not trigger inflammatory responses, thus highlighting their potential as anti-inflammatory agents.

Preparation of RGDS@NGQDs F127 Eye Drops and Their Intracellular Antioxidant Capacity

To increase the binding ability of NGQDs with corneal epithelium, NGQDs were chemically linked with RGDS peptides through amide bonding. The RGDS sequence is known for its interactions with a range of αv integrins, specifically $\alpha\text{v}\beta 1$, $\alpha\text{v}\beta 3$, $\alpha\text{v}\beta 5$, $\alpha\text{v}\beta 6$, and $\alpha\text{v}\beta 8$. Significantly, these αv integrins are highly expressed in the tear film of individuals suffering from DED, indicating a promising therapeutic target for NGQD-based treatments.^{30–32} Accordingly, RGDS peptides are expected to enhance the corneal permeability of quantum dots on the ocular surface, potentially improving therapeutic efficacy. The UV-Vis absorption spectrum of these RGDS-modified NGQDs displays a distinctive peak at 337 nm, which is clearly illustrated in Figure 5a. Moreover, the FT-IR spectrum, as depicted in Figure 5b, verified the successful

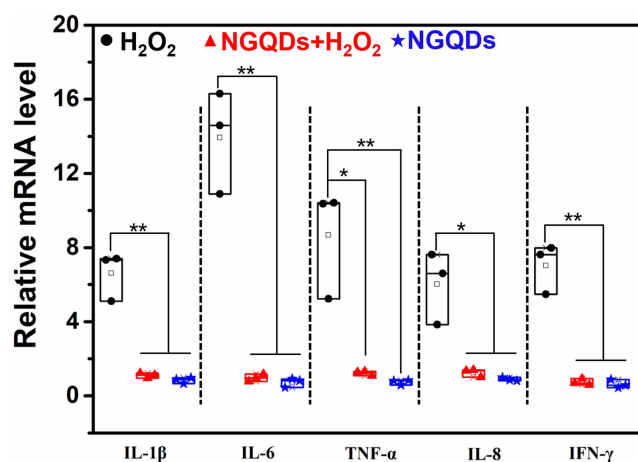


Figure 4 Relative expression of inflammation-related genes in HCECs. (* $p \leq 0.05$, ** $p \leq 0.01$ vs the corresponding treatment group linked with it).

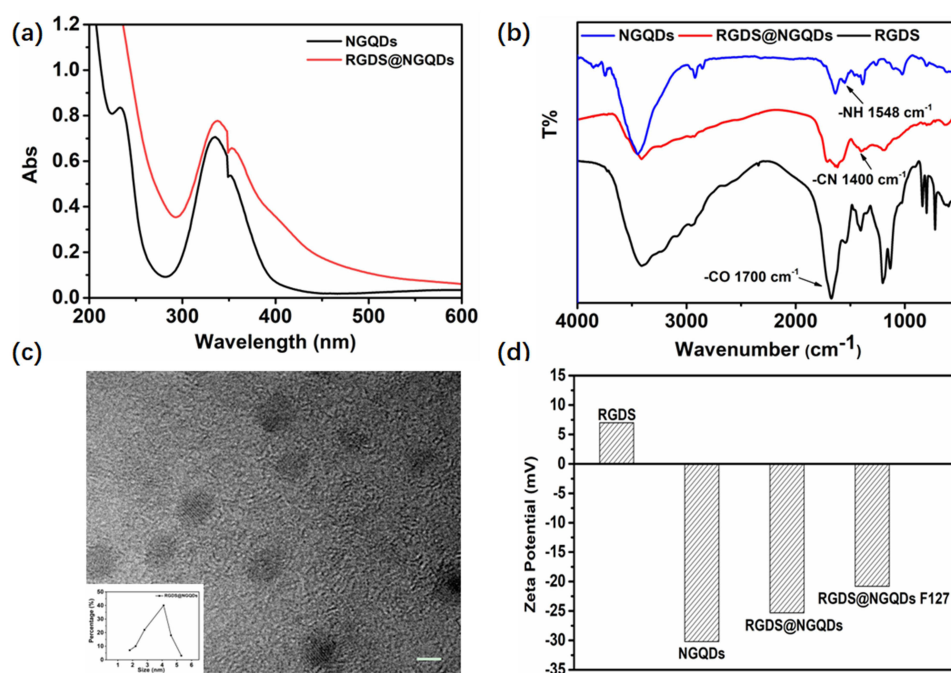


Figure 5 Characterization of RGDS@NGQDs. (a) UV-Vis spectra of NGQDs and RGDS@NGQDs; (b) FT-IR spectra of NGQDs, RGDS@NGQDs and RGDS; (c) HRTEM image of RGDS@NGQDs (Inset: the size distribution of RGDS@NGQDs); (d) The zeta potential of RGDS, NGQDs, RGDS@NGQDs and RGDS@NGQDs F127 by dynamic light scattering.

conjugation by showcasing the reaction between the amine groups of NGQDs (-NH_2 at 1548cm^{-1}) and the carboxyl groups of RGDS (-COOH at 1700cm^{-1}), culminating in the formation of an amide group (-CN at 1400cm^{-1}) within the RGDS@NGQDs complex. Observations using HRTEM revealed that the morphology and size of RGDS@NGQDs were similar to those of NGQDs, with good dispersibility (Figure 5c). After this confirmation, the lyophilized RGDS@NGQDs complex was dissolved in a 0.1% weight/volume (w/v) Pluronic F127 solution, leading to the preparation of the RGDS@NGQDs F127 eye drop formulation. We conducted zeta potential measurements for RGDS@NGQDs F127 eye drops and their precursor substances. Figure 5d illustrates that the zeta potential of RGDS is $+6.98\text{ mV}$, while that of NGQDs stands at -30.2 mV . Consequently, the introduction of RGDS reduces the electronegativity of RGDS@NGQDs, resulting in an adjusted zeta potential of -25.3 mV . Upon dispersion of RGDS@NGQDs in 0.1% F127, the effective zeta potential shifts to -20.8 mV . To assess the stability of the RGDS@NGQDs F127 eye drops, we stored them at room temperature for 96 h, during which we monitored changes in their zeta potential. According to Figure S5, the zeta potential of RGDS@NGQDs F127 demonstrated remarkable stability throughout the 96-h period.

To evaluate the effect of RGDS peptide modification on the cellular uptake of NGQDs, HCECs were co-cultured separately with NGQDs and RGDS@NGQDs ($200\text{ }\mu\text{g/mL}$) for 0.5 h or 2 h. It was observed that both materials were able to enter the cells (the blue fluorescence in Figure 6a). Notably, within just 0.5 h of incubation, the uptake of RGDS@NGQDs in cells was significantly higher than that of NGQDs. As the culture time extended to 2 h, there was no observed increase in the cellular uptake of NGQDs, but the uptake of RGDS@NGQDs in cells increased by ~ 2.6 times compared to 0.5 h (Figure 6b). Furthermore, the intracellular antioxidant efficacy of the RGDS@NGQDs was evaluated (Figure 6c). In the presence of H_2O_2 -induced oxidative stress, cell viability decreased to approximately 40%. However, when cells were co-cultured with RGDS@NGQDs, a significant increase in survival rates was observed. Notably, the viability of HCECs was restored to approximately 68% after 24 h of co-cultured with $10\text{ }\mu\text{g/mL}$ RGDS@NGQDs. This indicates that RGDS@NGQDs, even at lower concentrations, exhibit superior protection against oxidative stress compared to unmodified NGQDs (Figure 2b), primarily due to their higher cellular uptake. We further assessed the cytotoxic effects of RGDS@NGQDs on HCECs. Our findings revealed that at a concentration of $50\text{ }\mu\text{g/mL}$, RGDS@NGQDs led to a reduction in HCECs viability to 80%. This decrease in cell viability could be attributed to the

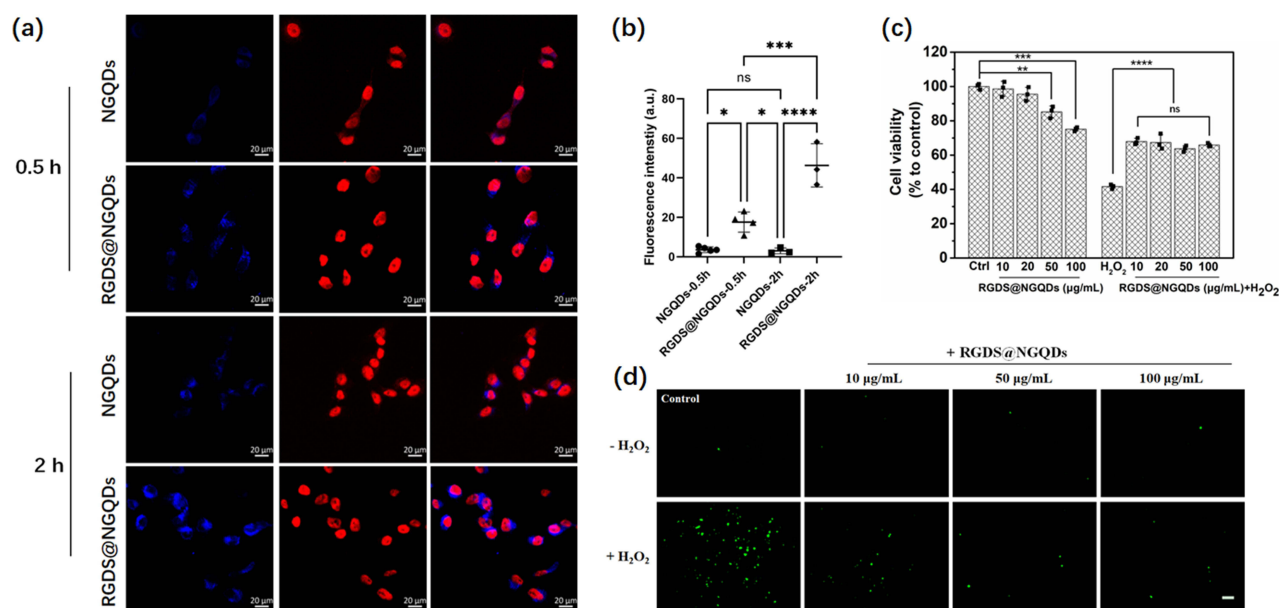


Figure 6 Cellular uptake and intracellular antioxidant capacity of RGDS@NGQDs. (a) Confocal microscopy observed the uptake of NGQDs or RGDS@NGQDs (200 µg/mL) in HCECs at 0.5 or 2 h incubations. Nuclei were stained with 7-AAD (Ex/Em: 546/647 nm, red fluorescence), NGQDs and RGDS@NGQDs excited at 370 nm showed blue fluorescence. Scale bar: 20 µm; (b) The intracellular fluorescence intensity of NGQDs or RGDS@NGQDs, quantified using Image J; (c) The cytocompatibility of RGDS@NGQDs and their antioxidant capacity, as assessed by CCK-8 assay; (d) ROS detection in HCECs by DCFH-DA probes; the scale bar represents 100 µm. (ns. $p > 0.05$, * $p \leq 0.05$, ** $p \leq 0.01$, *** $p \leq 0.001$, **** $p \leq 0.0001$ vs the corresponding treatment group linked with it).

potent antioxidant properties of RGDS@NGQDs, which potentially disrupts the redox equilibrium within the HCECs, consequently diminishing their viability. Subsequently, the DCFH-DA fluorescent probe was utilized to observe alterations ROS concentration in HCECs co-cultured with RGDS@NGQDs (Figure 6d). Upon stimulation with H₂O₂, a significant increase in green fluorescence was observed, indicating the production of ROS within the cells. When the cells were co-cultured with varying concentrations of RGDS@NGQDs, even under the stimulation of H₂O₂, the fluorescence intensity within the cells markedly decreased as the concentration of RGDS@NGQDs increased. This suggests that RGDS@NGQDs serve an antioxidative function within the cells. Additionally, it was noted that subsequent to the co-culture of cells with RGDS@NGQDs, there was less green fluorescence, suggesting that RGDS@NGQDs do not impart oxidative stress on the cells.

In vivo Therapeutic Effects of RGDS@NGQDs F127 Eye Drops

To evaluate the therapeutic efficacy of RGDS@NGQDs F127 eye drops in treating DED, we induced a DED mouse model using scopolamine hydrobromide injections.¹⁴ Animals suffering from DED were administered various treatments: PBS for the DED control group, NGQDs F127 eye drops for the NGQDs group (where NGQDs were lyophilized and subsequently reconstituted in 0.1% Pluronic F127 (w/v) to create NGQDs F127 eye drops), and RGDS@NGQDs F127 eye drops for the RGDS@NGQDs group. Following 7 days of treatment, the corneas from each group were evaluated using the corneal fluorescein staining score. This involved staining the corneas with fluorescent sodium, and subsequently examining them through slit-lamp microscopy, as depicted in Figure 7a. The damage on the corneal surface, when stained, exhibits green fluorescence. Relative to the healthy control group, the DED group demonstrated prominent plaque staining. However, following treatment with either NGQDs F127 or RGDS@NGQDs F127 eye drops, the corneas predominantly showed punctate or micropunctate staining. To quantify the effectiveness of these treatments for DED, fluorescein staining scores were assessed (Figure S6a). The fluorescein staining scores were 2.8 ± 1.4 for the healthy group and 12.3 ± 2.5 for the DED group; this marked increase in the score of the DED group, as compared to the healthy group, was statistically significant ($p \leq 0.001$). Post-treatment with the respective eye drops, the NGQDs group exhibited a score of 8.3 ± 1.7 , whereas the RGDS@NGQDs group demonstrated a lower score of 5.1 ± 2.3 . Notably, both treatment groups showed a significant decrease in scores compared to the DED group ($p \leq 0.001$). Furthermore, the score in the

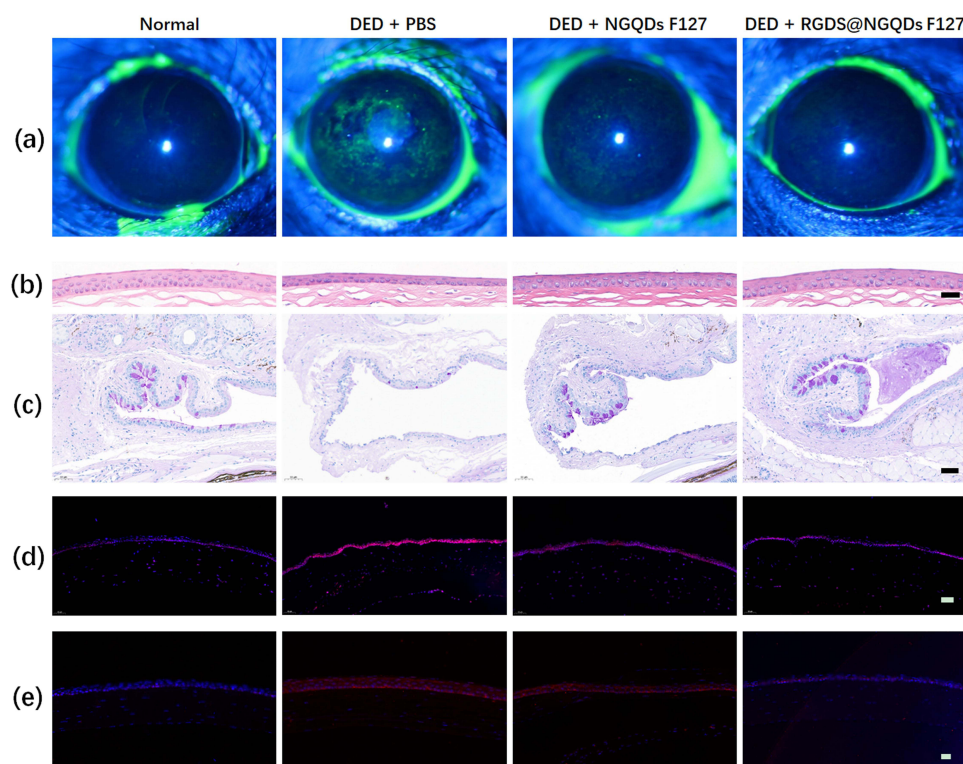


Figure 7 Representative diagnosis images of each group after 7 days of treatment. (a) fluorescein staining images; (b) histological images of corneas stained with H&E (scale bar: 50 μ m); (c) histological images of conjunctiva stained with PAS (scale bar: 50 μ m); (d) frozen sections of corneal tissue stained with DHE and DAPI (scale bar: 50 μ m); (e) IL-1 β detection by immunostaining on the corneal epithelial cells in the mice eyes after 7 days of treatment (scale bar: 20 μ m).

RGDS@NGQDs group was significantly reduced in comparison to the NGQDs group ($p \leq 0.01$). This suggests that the incorporation of RGDS peptides substantially enhances the therapeutic efficacy of NGQDs in treating DED.

After 7 days of treatment, in order to more thoroughly examine the corneal recovery, eyes from each group were harvested and subjected to H&E staining. Subsequently, the morphological characteristics of the cornea were meticulously observed under a microscope, as shown in Figures 7b and S6b. We observed that the corneal epithelium in the DED group had a reduced thickness of $12.67 \pm 0.45 \mu\text{m}$, which was markedly thinner and less densely arranged compared to the healthy group, in which the thickness measured $25.9 \pm 0.95 \mu\text{m}$. Additionally, there was a notable disorganization in the corneal stroma of the DED group. After 7 days of treatment using NGQDs F127 eye drops, noticeable healing was observed in the damaged corneas. The stromal structure showed signs of smoothing, and the thickness of the corneal epithelium increased to $20.73 \pm 1.3 \mu\text{m}$. Corneas treated with RGDS@NGQDs F127 eye drops showed a more remarkable normalization in morphology compared to those treated with NGQDs F127 eye drops. Following the RGDS@NGQDs F127 treatment, the corneal morphology displayed a recovery that closely resembled normal, healthy corneas, with an epithelial thickness of $23.08 \pm 0.3 \mu\text{m}$, and a similarly structured stroma.

Conjunctival goblet cells secrete mucins on the corneal epithelium, forming a part of the tear film and preventing tear evaporation of tears. A reduction in conjunctival goblet cells is a recognized characteristic of DED. We further utilized PAS staining to assess the density of conjunctival goblet cells in each group after the treatment (Figures 7c and S6c). Microscopic examination showed a marked reduction in the numbers of goblet cells in the PBS-treated group compared to the normal group ($p \leq 0.001$). In contrast, administration of NGQDs F127 or RGDS@NGQDs F127 eye drops resulted in a significant rebound in goblet cell density ($p \leq 0.05$ for NGQDs group and $p \leq 0.01$ for RGDS@NGQDs group). Remarkably, the RGDS@NGQDs F127-treated group displayed a denser population of goblet cells compared to the NGQDs F127-treated group, indicating a superior efficacy of RGDS@NGQDs F127 in replenishing these cells.

To evaluate the efficacy of eye drops in eliminating ROS, the corneas were frozen and sectioned for ROS analysis following a 7-day treatment period. The sections were then stained using DAPI and dihydroethidium (DHE), a probe that

reacts with ROS to emit red fluorescence. Microscopic observations (as depicted in Figure 7d) showed intense red fluorescence in the DED group, signifying high ROS production. Notably, in groups treated with either NGQDs F127 or RGDS@NGQDs F127 eye drops, a significant reduction in red fluorescence was observed, indicating a decrease in ROS levels. This reduction suggests a direct correlation between the eye drops' effectiveness in treating dry eye and their ROS-clearing capabilities. IL-1 β plays a critical role in mediating ocular surface inflammation in DED by triggering innate immune responses, and intensifying the inflammatory cascade, thereby worsening DED.¹¹ In comparison to the normal group, IL-1 β expression was significantly elevated in the DED group (Figure 7e). While the NGQDs F127 group still showed elevated levels of IL-1 β expression, it exhibited some inhibitory effects relative to the DED group. Notably, the RGDS@NGQDs F127 group demonstrated a significant reduction in IL-1 β expression, indicating the most potent suppression of inflammatory factor expression.

Discussion

Healthy tear fluid maintains a balance between the production and neutralization of ROS, particularly superoxide (O_2^-), hydrogen peroxide (H_2O_2), and hydroxyl radical ($\cdot OH$). Oxidative stress arises when this equilibrium is disrupted by an excess of ROS over antioxidants. It is widely recognized that such oxidative stress is a fundamental factor in the pathology of DED. A pivotal discovery of our study is the significant antioxidant activity of NGQDs. We found that, *in vitro*, NGQD treatment (i) enhances cell survival under oxidative stress conditions, and (ii) decreases the apoptosis rate in cells subjected to oxidative stress.

This study is predicated on the hypothesis that antioxidants targeting DED can function on two distinct levels. First, an antioxidant medication can directly scavenge ROS from the tear film. Second, such drugs may enhance or augment intracellular antioxidant mechanisms in cells vulnerable to ROS. Our observations indicate that the NGQDs used in this study operate effectively on both of these levels. Through TMB detection and total antioxidant capacity assays, we established that NGQDs can efficiently neutralize ROS in the medium. Further, DCFH-DA probe assays demonstrated a significant reduction in intracellular ROS levels due to NGQD intervention. We further observed an upregulation and nuclear translocation of Nrf2 in response to NGQD stimulation, suggesting an activation of the Nrf2-mediated antioxidant pathway in cells. These findings collectively underscore that NGQDs exert their antioxidant effects by both scavenging extracellular ROS and activating internal cellular antioxidant pathways.

The scope of the study was broadened to include an investigation into the inflammatory responses triggered by excessive oxidative stress. We observed that the transcription levels of inflammatory markers, including IL-1 β , IL-6, IL-8, TNF- α , and IFN- γ , were significantly elevated in HCEC cells following exposure to H_2O_2 . Notably, when these cells were treated with NGQDs, we observed a marked reduction in the transcription levels of these inflammatory cytokines, returning them to normal levels. This data suggests that NGQDs not only counteract oxidative stress, but also exhibit anti-inflammatory properties through their antioxidant activity.

The compelling outcomes of our *in vitro* experiments encouraged us to extend our research to *in vivo* studies, utilizing a mouse model of DED. To facilitate this transition, we made two key modifications to the NGQDs. The first alteration involved a structural modification: we synthetically coupled the tetrapeptide RGDS to the amino groups present on the surface of the NGQDs. This process resulted in the formation of quantum dots termed RGDS@NGQDs. The rationale behind this modification was to enhance the binding affinity of NGQDs to corneal epithelial cells, in order to increase the corneal permeability of the quantum dots on the ocular surface. The second modification involved a change in the dispersion medium for the quantum dots: instead of a cell growth medium, we used 0.1% Pluronic F127. This newly formulated variant treatment was subsequently re-evaluated through *in vitro* testing. When HCEC cells were subjected to oxidative stress (H_2O_2), their survival rate improved to 68% under the protection of RGDS@NGQDs F127 at a concentration of 10 $\mu g/mL$. This result suggests that RGDS@NGQDs F127 demonstrates superior antioxidant activity compared to the unmodified NGQDs. Following these encouraging results, we treated RGDS@NGQDs F127 as an eye drop therapy to treat DED in a mouse model over a period of seven days. The efficacy of the new RGDS@NGQDs F127 formulation was assessed by measuring several parameters and comparing them across different treatment groups: (i) healthy, untreated mice eyes; (ii) DED mice treated with PBS eye drops; and (iii) DED mice treated with NGQDs F127 eye drops. The assessed parameters included fluorescein staining scores, corneal morphology, goblet cell density, ROS and IL-1 β level on the corneal epithelial cells (both through histopathology). The experimental results indicate that RGDS@NGQDs F127 eye drops effectively ameliorated DED

symptoms by mitigating oxidative stress and relieving inflammation in the diseased eyes, outperforming the NGQDs F127 eye drops in this regard.

The study demonstrates that our technique for nitrogen doping and the addition of the RGDS tetrapeptide enhances the antioxidant properties of quantum dots. However, it is important to recognize that the eye contains various cell types, each with distinct responses to oxidative stress and unique mechanisms to combat ROS. The value of this research lies in its contribution to the understanding of DED pathology. Additionally, it offers potential for developing new quantum-dot-based antioxidant treatments for this condition.

Conclusion

The findings from this comprehensive in vitro and in vivo study reinforce the concept that antioxidant agents hold promise as a foundation for developing effective treatments for DED. Throughout our investigation, we prepared and analyzed NGQDs, demonstrating their dual-level activity as both effective scavengers of ROS in tear fluid, and as enhancers of intracellular antioxidant pathways. The performance of these NGQDs was further augmented by chemically attaching the RGDS tetrapeptide, resulting in RGDS-functionalized NGQDs (RGDS@NGQDs). Additionally, the suspension of RGDS@NGQDs in a 0.1% Pluronic F127 solution (RGDS@NGQDs F127) showed improved efficacy. In vivo tests using RGDS@NGQDs F127, conducted on a well-established mouse model of DED and compared with untreated DED mice, demonstrated that this agent, when applied as eye drops, effectively treats DED. This conclusion is drawn from a comprehensive set of experimental results, including fluorescein staining scores, corneal morphology, goblet cell density, and histopathological analysis. Overall, the findings of this study highlight the potential of nitrogen-doped GQDs, especially when chemically modified with RGDS and suspended in a suitable physical medium like Pluronic, in the development of innovative treatments for DED.

Abbreviations

DED, dry eye disease; ROS, reactive oxygen species; NGQDs, nitrogen-doped graphene quantum dots; HCECs, human corneal epithelial cells; (O_2^-), superoxide anion; H_2O_2 , hydrogen peroxide; $\cdot OH$, hydroxyl radicals; GQDs, Graphene quantum dots; Nrf2, Nuclear factor E2-related factor 2; RGDS, Arg-Gly-Asp-Ser; HRTEM, high-resolution transmission electron microscopy; AFM, atomic force microscopy; XPS, X-ray photoelectron spectroscopy; UV-Vis, ultraviolet-visible; FT-IR, Fourier transform infrared; TMB, 3,3',5,5'-Tetramethylbenzidine; HRP, horseradish peroxidase; FRAP, ferric reducing ability of plasma; Fe^{3+} -TPTZ, Ferric-tripyridyltriazine; FBS, fetal bovine serum; NC, negative control group; DCFH-DA, 2'-7'-dichlorofluorescein diacetate; RT-PCR, reverse transcription polymerase chain reaction; H&E, hematoxylin eosin; PAS, periodic acid-Schiff; DHE, dihydroethidium.

Acknowledgments

Financial supports for this work from the Zhejiang National Nature Science Foundation (LY20C100002, LQ21H120008), the Wenzhou Bureau of Science and Technology (Y20220150), the Medical and Health Technology Project in Zhejiang Province (2023RC088), the Agricultural and Social Development Science and Technology Plan Project in Yinzhou, Ningbo City (2023AS017), the Ningbo science and technology plan project (2023J211), the project of Ningbo Eye Hospital (2022QN002), the Zhejiang Medical and Health Science and Technology Project (No. 2023RC088), and the Yinzhou Agricultural and Social Development Scientific Research Project (2023AS017) are acknowledged.

Disclosure

The authors report no conflicts of interest in this work.

References

1. Tavakoli A, Flanagan JL. Dry eye disease: an (in)convenient truth. *Clin Exp Optom*. 2022;105(2):222–229. doi:10.1080/08164622.2021.1945410
2. Louie HH, Mugisho OO, Chamley LW, Rupenthal ID. Extracellular vesicles as biomarkers and therapeutics for inflammatory eye diseases. *Mol Pharm*. 2023;20(1):23–40. doi:10.1021/acs.molpharmaceut.2c00414
3. Huang L, Gao H, Wang Z, Zhong Y, Hao L, Du Z. Combination nanotherapeutics for dry eye disease treatment in a rabbit model. *Int J Nanomed*. 2021;16:3613–3631. doi:10.2147/IJN.S301717

4. Lu YT, Wu YQ, Zhou XJ, et al. Editorial: advances in the pathophysiology, diagnosis, and treatment of dry eye disease. *Front Med-Lausanne*. 2022;9:1 doi:10.3389/fmed.2022.925876.
5. Lou Q, Pan L, Xiang S, et al. Suppression of NLRP3/Caspase-1/GSDMD mediated corneal epithelium pyroptosis using melatonin-loaded liposomes to inhibit benzalkonium chloride-induced dry eye disease. *Int J Nanomed*. 2023;18:2447–2463. doi:10.2147/IJN.S403337
6. Luo L-J, Jian H-J, Harroun SG, Lai J-Y, Unnikrishnan B, Huang C-C. Targeting nanocomposites with anti-oxidative/inflammatory/angiogenic activities for synergistically alleviating macular degeneration. *Appl Mater Today*. 2021;24:1 doi:10.1016/j.apmt.2021.101156.
7. Tzong-Yun G, Tzong-Yun G, Tzong-Yun G, Lai J-Y. Biofunctionalization of nanoceria with sperminated hyaluronan enhances drug delivery performance for corneal alkali burn therapy. *Chem Eng J*. 2023;476:146864. doi:10.1016/j.cej.2023.146864
8. Yang C-J, Anand A, Huang C-C, Lai J-Y. Unveiling the power of gabapentin-loaded nanoceria with multiple therapeutic capabilities for the treatment of dry eye disease. *ACS Nano*. 2023;17(24):25118–25135. doi:10.1021/acsnano.3c07817
9. Wu DD, Lim BXH, Seah I, et al. Impact of microplastics on the ocular surface. *Int J Mat Sci*. 2023;24:1 doi:10.3390/ijms24043928.
10. Jung SJ, Mehta JS, Tong L. Effects of environment pollution on the ocular surface. *Ocul Surf*. 2018;16(2):198–205. doi:10.1016/j.jtos.2018.03.001
11. Li S, Lu Z, Huang Y, et al. Anti-oxidative and anti-inflammatory micelles: break the dry eye vicious cycle. *Adv Sci (Weinh)*. 2022;9(17):e2200435. doi:10.1002/advs.202200435
12. Le Gal K, Schmidt EE, Sayin VI. Cellular redox homeostasis. *Antioxidants*. 2021;11(1):10. doi:10.3390/antiox11010010
13. Yang CJ, Nguyen DD, Lai JY. Poly(l-histidine)-mediated on-demand therapeutic delivery of roughened ceria nanocages for treatment of chemical eye injury. *Adv Sci*. 2023;10(26):e2302174. doi:10.1002/advs.202302174
14. Lin PH, Jian HJ, Li YJ, et al. Alleviation of dry eye syndrome with one dose of antioxidant, anti-inflammatory, and mucoadhesive lysine-carbonized nanogels. *Acta Biomater*. 2022;141:140–150. doi:10.1016/j.actbio.2022.01.044
15. Lim JC, Suzuki-Kerr H, Nguyen TX. Redox homeostasis in ocular tissues: circadian regulation of glutathione in the lens? *Antioxidants*. 2022;12(1):11. doi:10.3390/antiox12010011
16. Nguyen DD, Luo LJ, Yang CJ, Lai JY. Highly retina-permeating and long-acting resveratrol/metformin nanotherapeutics for enhanced treatment of macular degeneration. *ACS Nano*. 2023;17(1):168–183. doi:10.1021/acsnano.2c05824
17. Awwad S, Ahmed AHAM, Sharma G, et al. Principles of pharmacology in the eye. *Brit J Pharmacol*. 2017;174(23):4205–4223. doi:10.1111/bph.14024
18. Li YJ, Luo LJ, Harroun SG, et al. Synergistically dual-functional nano eye-drops for simultaneous anti-inflammatory and anti-oxidative treatment of dry eye disease. *Nanoscale*. 2019;11(12):5580–5594. doi:10.1039/C9NR00376B
19. Luo LJ, Nguyen DD, Lai JY. Long-acting mucoadhesive thermogels for improving topical treatments of dry eye disease. *Mater Sci Eng C Mater Biol Appl*. 2020;115:111095. doi:10.1016/j.msec.2020.111095
20. Nguyen DD, Luo LJ, Lai JY. Thermogels containing sulfated hyaluronan as novel topical therapeutics for treatment of ocular surface inflammation. *Mater Today Bio*. 2022;13:100183. doi:10.1016/j.mtbio.2021.100183
21. Seen S, Tong L. Dry eye disease and oxidative stress. *Acta Ophthalmol*. 2018;96(4):E412–E420. doi:10.1111/aos.13526
22. Wu Z, Pan T, Lin D, et al. Biocompatible tumor-targeted GQDs nanocatalyst for chemodynamic tumor therapy. *J Mater Chem B*. 2022;10(18):3567–3576. doi:10.1039/D1TB02734D
23. Jian H-J, Ren-Siang W, Lin T-Y, et al. Super-cationic carbon quantum dots synthesized from spermidine as an eye drop formulation for topical treatment of bacterial keratitis. *ACS nano*. 2017;11(7):6703–6716. doi:10.1021/acsnano.7b01023
24. Lin H-Y, Wang S-W, Mao J-Y, et al. Carbonized nanogels for simultaneous antibacterial and antioxidant treatment of bacterial keratitis. *Chem Eng J*. 2021;411:1 doi:10.1016/j.cej.2021.128469.
25. Dehvari K, Chiu SH, Lin JS, Girma WM, Ling YC, Chang JY. Heteroatom doped carbon dots with nanoenzyme like properties as theranostic platforms for free radical scavenging, imaging, and chemotherapy. *Acta Biomater*. 2020;114:343–357. doi:10.1016/j.actbio.2020.07.022
26. Zhao L, Wang YM, Li Y. Antioxidant activity of graphene quantum dots prepared in different electrolyte environments. *Nanomaterials-Basel*. 2019;9:1 doi:10.3390/nano9121708.
27. Ruiz V, Yate L, Garcia I, Cabanero G, Grande HJ. Tuning the antioxidant activity of graphene quantum dots: protective nanomaterials against dye decoloration. *Carbon*. 2017;116:366–374. doi:10.1016/j.carbon.2017.01.090
28. Choudhary P, Biswas S, Kandoth N, et al. Graphene quantum dots alleviate ROS-mediated gastric damage. *iScience*. 2022;25(4):104062. doi:10.1016/j.isci.2022.104062
29. Wang HB, Zhang ML, Ma YR, et al. Carbon dots derived from citric acid and glutathione as a highly efficient intracellular reactive oxygen species scavenger for alleviating the lipopolysaccharide-induced inflammation in macrophages. *Acs Appl Mater Inter*. 2020;12(37):41088–41095. doi:10.1021/acsaami.0c11735
30. Ho TC, Yeh SI, Chen SL, Tsao YP. Integrin alpha v and vitronectin prime macrophage-related inflammation and contribute the development of dry eye disease. *Int J Mol Sci*. 2021;23(1):22. doi:10.3390/ijms23010022
31. Chen L, Deng J, Ailing Y, et al. Drug-peptide supramolecular hydrogel boosting transcorneal permeability and pharmacological activity via ligand-receptor interaction. *Bioact Mater*. 2022;10:420–429. doi:10.1016/j.bioactmat.2021.09.006
32. Pierschbacher MD, Ruoslahti E. Cell attachment activity of fibronectin can be duplicated by small synthetic fragments of the molecule. *Nature*. 1984;309(5963):30–33. doi:10.1038/309030a0
33. Ensign LM, Tang BC, Wang YY, et al. Mucus-penetrating nanoparticles for vaginal drug delivery protect against herpes simplex virus. *Sci Transl Med*. 2012;4:1 doi:10.1126/scitranslmed.3003453.
34. Mert O, Lai SK, Ensign L, et al. A poly(ethylene glycol)-based surfactant for formulation of drug-loaded mucus penetrating particles. *J Control Release*. 2012;157(3):455–460. doi:10.1016/j.jconrel.2011.08.032
35. Yu MR, Xu L, Tian FL, et al. Rapid transport of deformation-tuned nanoparticles across biological hydrogels and cellular barriers. *Nat Commun*. 2018;9:1 doi:10.1038/s41467-018-05061-3.
36. Li L, Li SH, Wang S, et al. Antioxidant and anti-glycated TAT-modified platinum nanoclusters as eye drops for non-invasive and painless relief of diabetic cataract in rats. *Chem Eng J*. 2020;398:1 doi:10.1016/j.cej.2020.125436.
37. Qi L, Th P, Li O, et al. Biocompatible nucleus-targeted graphene quantum dots for selective killing of cancer cells via DNA damage. *Commun Biol*. 2021;4(1):4. doi:10.1038/s42003-020-01536-6

38. Liu XF, Hao JL, Xie T, et al. Nrf2 as a target for prevention of age-related and diabetic cataracts by against oxidative stress. *Aging Cell*. 2017;16(5):934–942. doi:10.1111/ace.12645
39. Ayu Y, Zm L, Gt C, Sd H, Hs Y. Bamboo leaf flavonoids extracts alleviate oxidative stress in HepG2 cells via naturally modulating reactive oxygen species production and Nrf2-mediated antioxidant defense responses. *J Food Sci*. 2019;84(6):1609–1620. doi:10.1111/1750-3841.14609

International Journal of Nanomedicine

Dovepress

Publish your work in this journal

The International Journal of Nanomedicine is an international, peer-reviewed journal focusing on the application of nanotechnology in diagnostics, therapeutics, and drug delivery systems throughout the biomedical field. This journal is indexed on PubMed Central, MedLine, CAS, SciSearch®, Current Contents®/Clinical Medicine, Journal Citation Reports/Science Edition, EMBase, Scopus and the Elsevier Bibliographic databases. The manuscript management system is completely online and includes a very quick and fair peer-review system, which is all easy to use. Visit <http://www.dovepress.com/testimonials.php> to read real quotes from published authors.

Submit your manuscript here: <https://www.dovepress.com/international-journal-of-nanomedicine-journal>